scientific reports

Check for updates

OPEN

Impact of tellurium anion distribution depending on doping concentration and substrate temperature on the photovoltaic performance of Cu(In,Ga)Se_2 thin film solar cells

Semih Agca[1,2]✉, Hasan Arif Yetkin[3], Savas Sonmezoglu[4] & Guven Cankaya[1]

We explored how tellurium (Te) anion distribution as a function of doping concentration and substrate temperature effects on the photovoltaic (PV) performance of narrow-bandgap Cu(In, Ga)Se_2 thin film solar cells grown by a three-stage co-evaporation process. At low and moderate substrate temperatures (480 ℃ and 550 ℃), the inclusion of Te anions in the structure has negative impacts on photovoltaic parameters due to formation of disorder in the crystal structure, the deepening of the notch in the *GGI* gradient and the increase of defect-assisted recombination. At high substrate temperature (620 ℃), conversely, the presence of Te not only serves to improve the crystal structure and mitigate recombination through defect suppression but also facilitates the growth of large grains and attains a near-optimal *GGI* ratio (0.3) with a better gradient, which has a beneficial impact on the PV performance. These results highlight the role of Te anion distribution on PV performance of Cu(In, Ga)Se_2 thin film solar cells and its potential for highly efficient commercial thin-film solar cells in reasonable and effective ways as a function of substrate temperature and doping concentration.

Keywords Cu(In,Ga)$(Se,Te)_2$, Thin film, Solar cell, GGI gradient, Three-stage co-evaporation

Chalcopyrite type Cu(In, Ga)Se_2 (CIGSe) thin films have been studied by many research groups for solar cell applications. These materials are seen one of promising candidates as a thin film absorbing layer for thin film-based photovoltaic technology owing to tunable direct bandgap, high efficiency, stability, and effective usage of raw materials[1–4]. The achievement of high efficiency in CIGSe solar cell devices hinges upon establishing an optimal bandgap gradient within the CIGSe absorber layer[5,6]. One of the most important steps is to optimize the depth and type of the gradient, as an incompatible bandgap gradient might lead to a decline in PV performances[7]. This can be achieved by adjusting the [Ga]/([Ga]+[In]) (GGI) ratio to tune the bandgap between 1.04 and 1.67 eV, with the assistance of the presence of Na, which also serves to accelerate the interdiffusion of In and Ga[8,9]. Even though a bandgap of 1.45 eV is achieved at *GGI* ratios of 0.8 to obtain theoretically high-efficiency wide bandgap CIGSe solar cells[5], it has been reported that bandgaps of absorber layers in the range of 1.1–1.3 eV are achieved with the highest efficiency in these cells when the *GGI* ratio is between 0.25 and 0.30[10]. The substitution of anion elements exhibits similar behavior, and it is evident that the bandgap will change when Se is substituted for Te or S[11]. Undoubtedly, the main reason for variation in the bandgap gradient is related to the diffusion of cation (Ga and In) and/or anion (Se, S and Te) elements within the absorber layer, which is accomplished by controlling sources fluxes during a three-stage co-evaporation process. For this reason, the element diffusion within absorber layer process greatly depends not only on the rates of element concentration but also on the optimization of substrate temperature in a three-stage co-evaporation process.

[1]Department of Metallurgical and Materials Engineering, Faculty of Natural Sciences and Engineering, Ankara Yıldırım Beyazıt University, 06010 Ankara, Turkey. [2]Institute of Physics, Martin Luther University Halle-Wittenberg, 06120 Halle (Saale), Germany. [3]Department of Physics and Materials Science, University of Luxembourg, 4422 Belvaux, Luxembourg. [4]Department of Metallurgical and Materials Engineering, Karamanoglu Mehmetbey University, 70100 Karaman, Turkey. ✉email: semihagca@aybu.edu.tr

Despite the fact that there are numerous researches on the deposition of $CuInTe_2$[12–14], Cu(In, Ga)Te_2[15,16], and Cu(In, Ga)$(Se, Te)_2$[17–21] thin films using different techniques and the evaluation of their physical properties, there are relatively few studies on the photovoltaic properties of $CuInTe_2$ and $CuIn(Se, Te)_2$ based solar cells[22–24] compared to sulfur-based cells. The primary goal of Te incorporation in such experiments was to reduce the bandgap of the absorber layer, allowing it to be used as a bottom cell in multi-junction solar cells[25]. Nevertheless, these works have demonstrated that low amounts of Te doping into the CIGSe structure will be enough to tune the GGI gradient, which effectively control the bandgap gradients of the solar cells[26]. Moreover, it has been reported that the *GGI* ratio should be lowered below 0.3 for low substrate temperatures but should not be higher than 0.3 for high substrate temperatures while producing narrow-bandgap tellurium doped CIGSe solar cells[27]. It has also been shown that the tellurium atomic ratios of narrow-bandgap CIGSeTe solar cells above 1.4% cause surface cracks due to high stress caused by lattice distortion[28]. However, direct proof of these effects remains a challenge, since their practical implications for the material and device performance are not yet fully understood. Herein, we developed CIGSeTe thin film-based solar cells using three-stage co-evaporation to further understand the impacts of low Te amount and substrate temperature on the *GGI* gradient and photovoltaic characteristics of thin film solar cells. Based on experimental findings, increasing the amount of Te anion at 480 and 550 ℃ substrate temperatures significantly degrades photovoltaic performance, whereas increasing the amount of Te anion at 620 ℃ substrate temperature improves photovoltaic properties due to shift of *GGI* to 0.3 with a better gradient, the enhancement of grain size and crystallite by the incorporation of Te into the structure and suppression of defects (gallium/indium/selenium interstitial and/or vacancies). These results will shed light on improving photovoltaic performances in CIGSe-based solar cells by adjusting the *GGI* gradient with poor Te concentration over 600 ℃ substrate temperatures in the three-stage co-evaporation process.

Experimental details

CIGSeTe thin films were deposited on molybdenum (~400 nm) coated soda lime glass (SLG) by a three-stage co-evaporation process under vacuum atmosphere with a background pressure of $2{\cdot}10^{-7}$ mbar. Since there was no diffusion barrier between SLG and Mo, Na could diffuse from SLG through Mo into the absorber layer during the deposition. The co-evaporation process was performed in a multi-source chamber equipped with a laser light scattering to control the composition and thickness of the deposited film in-situ. The first stage of the co-evaporation process was started by In and Ga evaporation. Cu was only deposited in the 2nd stage. In the third stage, In and Ga were evaporated until a Cu-poor stoichiometry was achieved. After the 3rd stage, NaF was deposited with an evaporation rate of 0.1 Å/s for 600 s without breaking the vacuum[10]. Elemental Se was evaporated (above the melting point of 220 ˚C) and Te was sublimated (below the melting point of 450 ˚C) simultaneously during the co-evaporation process and the NaF post deposition. The temperatures of the Se and Te sources were set between 240 and 260 ˚C and 370–400 ˚C, respectively, to obtain different [Te]/([Te]+[Se]) (*TTS*) ratios, while the flux ratio of ([Te]+[Se])/[metals] kept constant at about 10. Samples with different substrate temperatures and Te contents were studied in a systematical approach. An overview of the samples is given in Table 1.

The numbers 480, 550, and 620 in the sample names represent the substrate temperatures (T_{Sub}) of 480 ˚C, 550 ˚C, and 620 ˚C, respectively. As in other studies, where the same evaporation system was used[29], it is estimated that the actual temperature under vacuum is 60 °C below the adjusted temperature. Samples denoted with 0 following the temperature value were prepared without Te. The number 0.6 represents ~0.6 at % of Te, corresponding to [Te]/([Te]+[Se]) ratio (*TTS*) of 0.011 ± 0.001, determined by energy dispersive X-ray spectroscopy at 15 kV acceleration voltage. Samples with the number 0.9 contain ~0.9 at % of Te, corresponding to *TTS* = 0.017 ± 0.001. *GGI* values of the samples were approximately 0.3, and Cu/(Ga + In) (*CGI*) values were in the range of 0.87–0.92.

The CIGSeTe absorber layers have a thickness of ~2 µm. Note that the samples have not been etched or washed prior to buffer layer. On top of them, ~50 nm of CdS were deposited via chemical bath deposition, followed by ~100 nm intrinsic ZnO (i-ZnO) and 200 nm indium tin oxide (ITO), deposited by sputtering. A Ni/Al/Ni front contact was evaporated by means of e-beam evaporation to complete the solar cells. Note that no

Sample	T_{Sub} (˚C)	E_g (eV)[a]	E_g (eV)[b]	Te/(Te + Se)	Ga/(Ga + In)	Cu/(Ga + In)
480-0	480	1.09	1.08	0.000	0.28	0.91
480 – 0.6	480	1.10	1.05	0.011	0.25	0.87
480 – 0.9	480	1.09	1.03	0.016	0.25	0.90
550-0	550	1.10	1.11	0.000	0.27	0.92
550 – 0.6	550	1.08	1.15	0.010	0.28	0.90
550 – 0.9	550	1.07	1.19	0.017	0.25	0.91
620-0	620	1.09	1.15	0.000	0.24	0.88
620 – 0.6	620	1.08	1.13	0.012	0.31	0.92
620 – 0.9	620	1.06	1.11	0.018	0.34	0.90

Table 1. Overview of elemental compositions from EDX and bandgap values extracted from UV-Vis spectra and *EQE* spectra. [a]Energy bandgap (eV) values were obtained from UV-Vis spectra. [b]Energy bandgap (eV) values were extracted from normalized *EQE* spectra.

anti-reflection coating was applied. Each sample has been mechanically scribed to have four solar cells with an active cell area of 0.5 cm^2.

The morphology and elemental composition analysis were performed by a ZEISS Supra 40 VP scanning electron microscope (SEM) with 5 kV acceleration voltage. X-ray diffraction (XRD) analysis was performed using a Rigaku Miniflex 600 XRD with CuKα radiation at 2θ values of 25˚ to 75˚. Each CIGSeTe absorber layer was also deposited on SLG without Mo back contact to eliminate the Mo peaks in XRD measurements and evaluate the thin films' optical characteristics. Absorption measurements were carried out between wavelengths of 800–1400 nm using a Shimadzu UV-2600 UV-Vis spectrophotometer. The samples were subjected to glow discharge optical emission spectroscopy (GDOES) using the Spectruma GDA750 instrument to obtain elemental in-depth profiles, as described in[30]. As we only have one reference sample containing a small amount of tellurium (0.06 at %), this reference sample was tried as a calibration sample in the quantification of the GDOES profiles. No smoothing treatment was applied to the surface and the quantification of tellurium in our samples is probably insufficient due to a much higher amount of tellurium than in the calibration sample. Current density – voltage (*J-V*) measurements of our cells were performed under AM1.5G standard test conditions at room temperature. A Xenon lamp equipped with a monochromator was used to measure the external quantum efficiency (*EQE*) by the lock-in method. The short circuit current (J_{SC}) was determined by the integration of *EQE* response with the AM1.5G spectrum. Power conversion efficiencies (η) of our cells were calculated using V_{OC} and *FF* from *J-V* measurement and J_{SC} from *EQE* measurement.

Results and discussion

The top-view and cross-sectional SEM images of thin films with varying Te concentrations and deposition temperatures are displayed in Fig. 1. The average grain sizes of the samples in the 480 ℃ deposition temperature are almost similar after Te incorporation. Since the estimated actual T_{Sub} for these samples is 420 ℃, which is below the melting point of Te, there is no liquid phase assisted crystallization. Hence, the incorporation of Te anion at temperatures lower than its melting point has no effect on grain size. No significant change was detected in the grain sizes, when the depositions occur at 550 ℃ with varying Te concentrations even though the actual T_{Sub} is 490 ℃ higher than melting point of Te. However, further increase in T_{Sub} (at 620 ℃) results in bigger grain sizes for both CIGSe and CIGSeTe thin films. The grain size difference at high temperature can be explained by a better promotion of liquid phase assisted crystallization by Te compared to Se, implying that the Te anion acts as nucleation centers to facilitate the grain growth of the absorber layer[26,31]. Overall, in order to take advantage effectively of liquid phase crystallization, deposition temperature must be sufficiently higher than the melting point of Te. Cross-sectional images of the samples are located on the right side in Fig. 1. The layer morphology was not significantly affected by different Te concentrations and/or *GGI* ratios and/or substrate temperatures, as demonstrated by the highly reproducible layer thickness of ~2 µm achieved through a three-stage co-evaporation process. At high substrate temperature (620 ℃) it is evident that the incorporation of Te significantly increased the grain size. In cases when the substrate temperature exceeds melting point of Te, this is consistent with the literature[24,26].

XRD spectra of all thin films on soda-lime glass are displayed in Fig. 2. The diffraction peaks of samples without Te can be indexed to the Cu(In, Ga)Se_2 with a *GGI* of 0.3 (JCPDS 00-035-1102). Since there is no JCPDS reference for CIGSeTe compound, calculation of peak positions by using data for CIGSe and CISeTe is considered as a reference. All samples exhibit a single phase with a highly preferred (112) orientation. Taking this prominent peak into consideration, it is obvious that the degree of distortion in the lattice rises with increasing Te concentrations at substrate temperatures below 550 ℃, resulting in a weakening of crystallinity. A distinct split is clearly seen in this main peak with increasing Te concentrations; however, this split disappears completely with an increasing in substrate temperature about 620 ℃. The underlying mechanism for this possible scenario can be explained by the reaction kinetics between Te and other elements as follows: Since the boiling point of Te is high (988 ℃ at atmospheric pressure), the applied vacuum pressure and T_{Sub} are not sufficient for Te to undergo ionization and turn into the formation of free ion. Therefore, since the Te is in the presence of a neutral species at low temperatures, the Te neutral species (atom), whose diffusion rate decrease according to Fick's first law, prefers to react with the Ga ions rather than the In ions which is rapidly moving to the Mo surface, implying that it promotes the formation of Cu-Ga/(Se-Te) phases, in agreement with the $CuGaTe_2$ secondary peaks seen in the magnified spectra in Fig. 2a. On the other hand, the drop in *GGI* ratios in Table 1 confirms the concept of a decrease in the quantity of Ga in the reaction environment because of Te element's interaction with Ga. On the other hand, Te can easily evaporate, particularly at the substrate temperature of 620 ℃, probably owing to above the boiling point of Te at applied vacuum pressure, and thereby becomes a free ion. This leads to the formation of Cu-In-Ga/(Se-Te) phases by capturing Ga and In ions inside bulk rather than surface due to increased diffusion rates. Thus, it not only improves crystallinity by lowering Cu/Ga/In deficiencies induced by Se vacancy during phase formation as seen Figs. 2b and c, but also promotes grain size by slowing down nucleation. Taking into account on the larger ionic radii of Te (221 pm) than Se (198 pm) ions, a reasonable shift in the (112) main peak toward the higher angle was observed with an increase in Te dopants in the absorber thin film, as illustrated in the inset of Fig. 2c, implying that Te anions are replaced with Se and act as an interstitial impurity in the thin film at T_{Sub} of 620 ℃[26].

The extracted E_g from UV-Vis can be seen in Fig. 3; Table 1 presents a summary of these findings in relation to E_g derived from *EQE*. According to Table 1, no acceptable variation in E_g obtained from both techniques was observed with the increase in substrate temperature. While variation of Te quantity and E_g value do not significantly correlate at temperatures below 500 ℃, conversely, a reduction in the bandgap was found along with an increment in Te above 620 ℃, which is consistent with earlier research in the literature[25,32]. This can be explained by the tellurium incorporation creating a new shallow energy level in the bandgap, which causes the valence band to shift upwards[33–36]. These findings exhibited a similar effect on the *GGI* gradient, which is directly

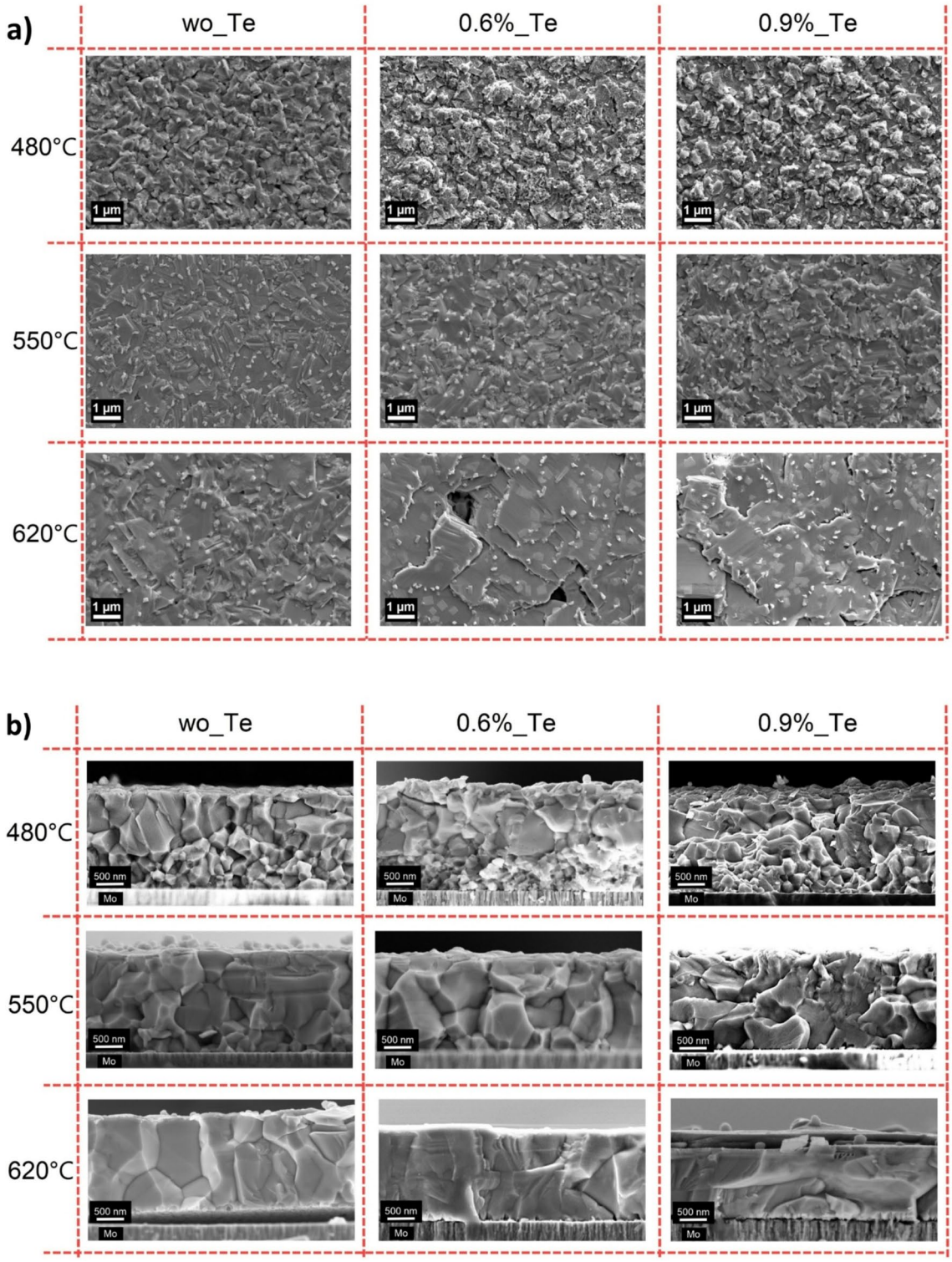

Fig. 1. (**a**) Top-view SEM and (**b**) Cross-sectional images of CIGSe and CIGSeTe thin film absorber layers with at varying substrate temperature on Mo-coated SLG substrate.

affected by the E_g gradient. At 620 ℃, increasing Te concentration raises the *GGI* value towards the ideal ratio (0.3) at which high efficiency is achieved; as expected, decreasing E_g with increasing *GGI* value is also verified in good agreement with the literature[1,37].

As can be seen from Fig. 4, *GGI* gradient flattens as T_{Sub} increases. Te incorporation at 480 ℃ made the notch of the *GGI* gradient deeper, indicating further slowing down the Ga diffusion throughout the absorber. The incorporation of Te at 550 ℃ appears to result in a less pronounced attenuation of Ga-diffusion than that

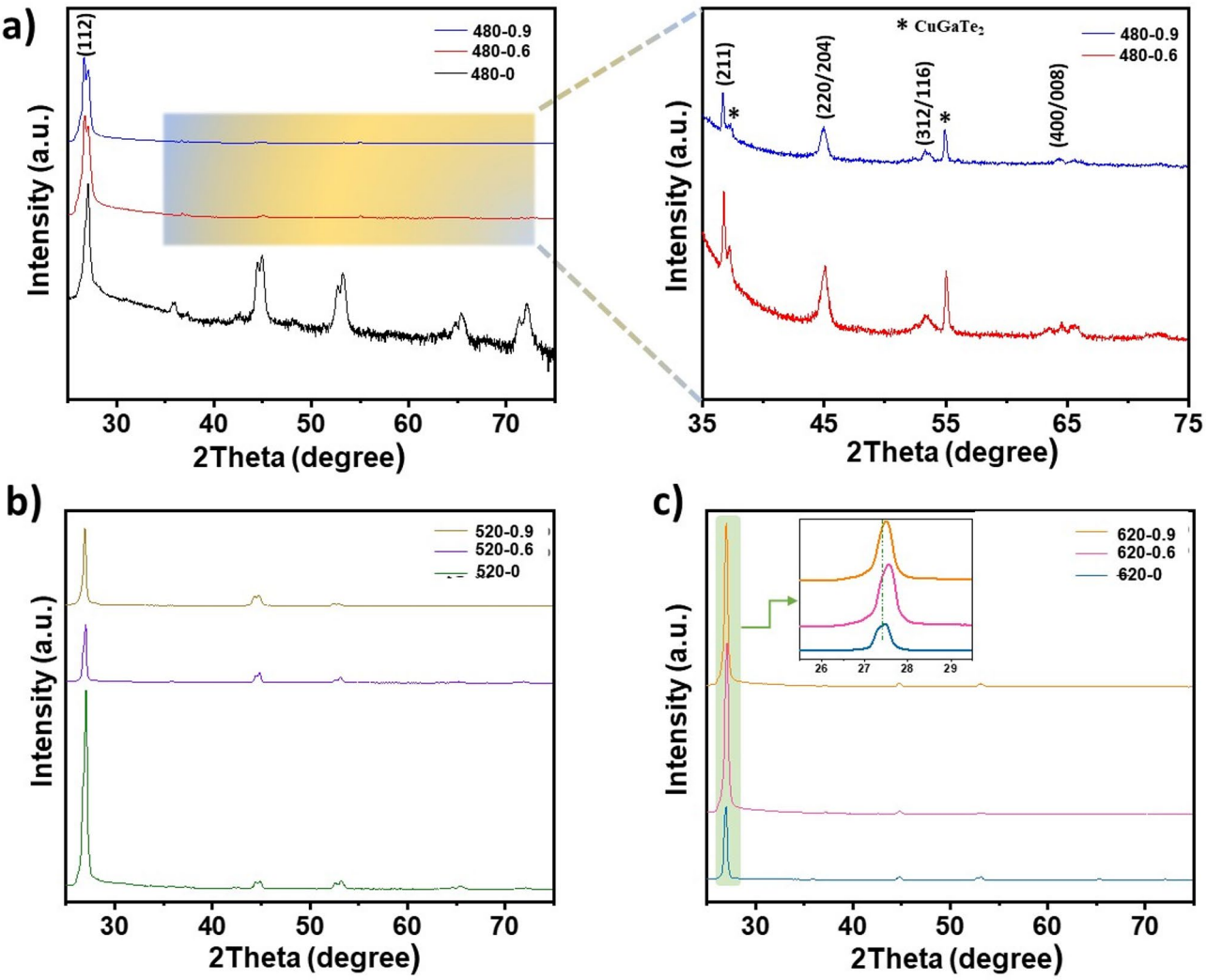

Fig. 2. The logarithmic X-ray diffraction (XRD) graphs of the thin films prepared at (**a**) T_{Sub} of 480 ℃ (**b**) T_{Sub} of 520 ℃, and (**c**) T_{Sub} of 620 ℃.

observed for the T_{Sub} of 480 ℃. On the other hand, highest T_{Sub} of 620 ℃ gives rise to changes in the gradient type from double to back surface gradient. It can be said that the addition of Te prevents Ga diffusion at low temperatures, while it promotes the diffusion of Ga at higher temperatures. This mechanism can be explained not only by the above-mentioned scenarios based on kinetic reactions, but also by the formation of larger grains through liquid phase-assisted crystallization, which reduces the number of grain boundaries and allows easier diffusion of Ga. The shape of the *GGI* gradient in CIGSe samples was found to be in good agreement with the literature at similar substrate temperatures[29,38].

To identify the impacts of relevant variables on performance of thin film solar cells, we displayed the statistical distribution of power conversion efficiency (PCE) per 10 devices in total in Fig. 5a. The PCE statistics presented in this figure indicate that the devices yield highly reproducible results. Figure 5b shows the PV performances of the best-performing thin film solar cells. Increasing the T_{Sub} enhanced the solar cell characteristics of Te-based $CIGSe_2$ cells, no effect was observed in Te-free cells. However, it was discovered that incorporation of Te into CIGSe exhibited negative effects on PV parameters such as V_{OC}, *FF* and J_{SC} at T_{Sub} below 550 ℃. This poorer performance may have originated from the high ideality factor, enhanced non-radiative recombination induced by defects, low carrier collection as a result of the less amount of Ga in the region close to the back contact due to preventing diffusion of Ga ions by interaction with Te on absorbing layer surface, and low *GGI* gradient inhibiting electron transport[5,9,39]. At 620 ℃, however, V_{OC} and *FF* increase with Te incorporation, whereas J_{SC} drops with a similar trend. These parameters of the best solar cells for all samples are shown in Table 2. Possible mechanisms underlying the enhanced device performance are the suppressing the defect in GBs through larger grain sizes, leading to higher *FF* and formation of shallow trap centers into the bandgap inhibiting non-radiative recombination, resulting in higher V_{OC} [40,41] On the other hand, the decrease in J_{SC} can be explained by the back surface gradient occurring upon Te incorporation[39]. Te incorporation into CIGSe at 620 ℃ is beneficial for device performance; however, decrease of Te content under 0.9% can negatively impact

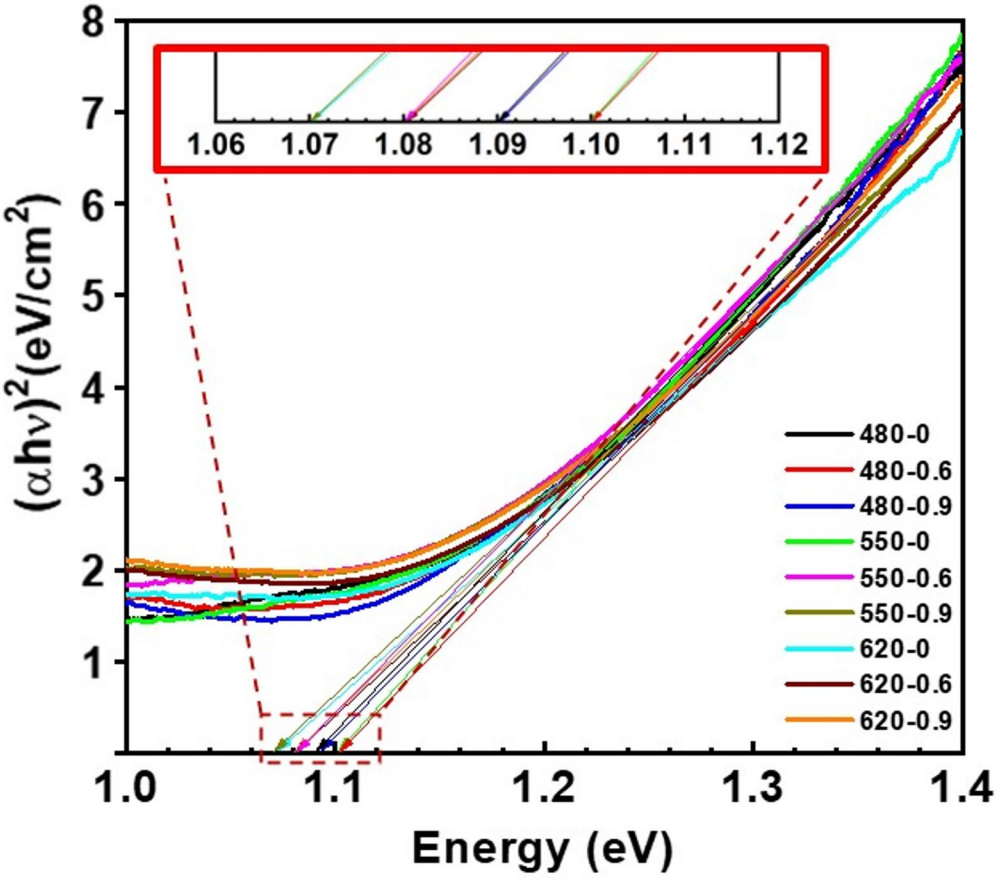

Fig. 3. Determination of optical direct bandgap of all samples deposited on SLG from UV-Vis absorption spectra.

its operation. Consequently, we will focus on research on high T_{Sub} (>600 ℃) and excess Te concentrations (between 1% and 1.4%) in the future to fabricate highly efficient Te-doped CIGSe solar cells.

To highlight the beneficial impact of Te and T_{Sub} variation on the bandgap gradient of CIGSe, External Quantum Efficiency (*EQE*) measurements of all devices were performed in Fig. 5c. The carrier collection in the range of 800 to 1100 nm is reduced for the Te-based cells, evidently attributable to the lower carrier collection caused by the *GGI* back surface gradient[39]. A wavelength independent increase of the *EQE* was observed for increasing T_{Sub} in CIGSeTe samples. However, the temperature change had a negligible impact on the *EQE* of CIGSe samples.

To demonstrate how the relevant variables dominate the *J-V* response of the devices at varying voltages, we presented dark *J-V* characteristics for all devices in Fig. 5d. At low voltages (Region I), the JV characteristics are predominantly influenced by shunt resistance (R_{sh}), at intermediate voltages (Region II) by the diode parameters, namely the ideality factor (n); and at high voltages (Region III) by series resistance (R_s). Taking into account the temperature-dependent changes in the regions, we observed a rise in the R_{sh}, a decrease in the R_s and a similar pattern in the slope of the current in the exponential second regime as the T_{sub} increased, implying that the devices display a much lower reverse current, a larger forward current due to high mobility, and lower non-radiative recombination rate due to less deep traps, high charge carriers injection. Surprisingly, we can say that the incorporation of tellurium generally leads to a negative trend in these parameters except for the application at high temperatures and high concentrations. We anticipate that our findings will serve as a roadmap for future research on higher substrate temperatures and tellurium concentrations.

Conclusions

We successfully revealed Te concentrations and substrate temperatures impacts on photovoltaic performances of CIGSe solar cells grown by three-stage co-evaporation process. Te incorporation disrupts the crystal structure, deepens the notch in the *GGI* gradients by suppressing Ga diffusion, and creates defects encouraging non-radiative recombination, and hence it has negative effects on photovoltaic performances at T_{Sub} below its boiling point (<600 ℃). When T_{Sub} more than 600 ℃, it is obvious that Te incorporation not only improves crystal structure and suppresses recombination by decreasing defects, but it also promotes large grain size and near-ideal *GGI* ratios (0.3) with a better gradient. Compared to Te-based CIGSe solar cells, optimum Te concentration (0.9%)-based cell at 620 ℃ exhibited the highest efficiency of 11.2%. Even though a full description of the

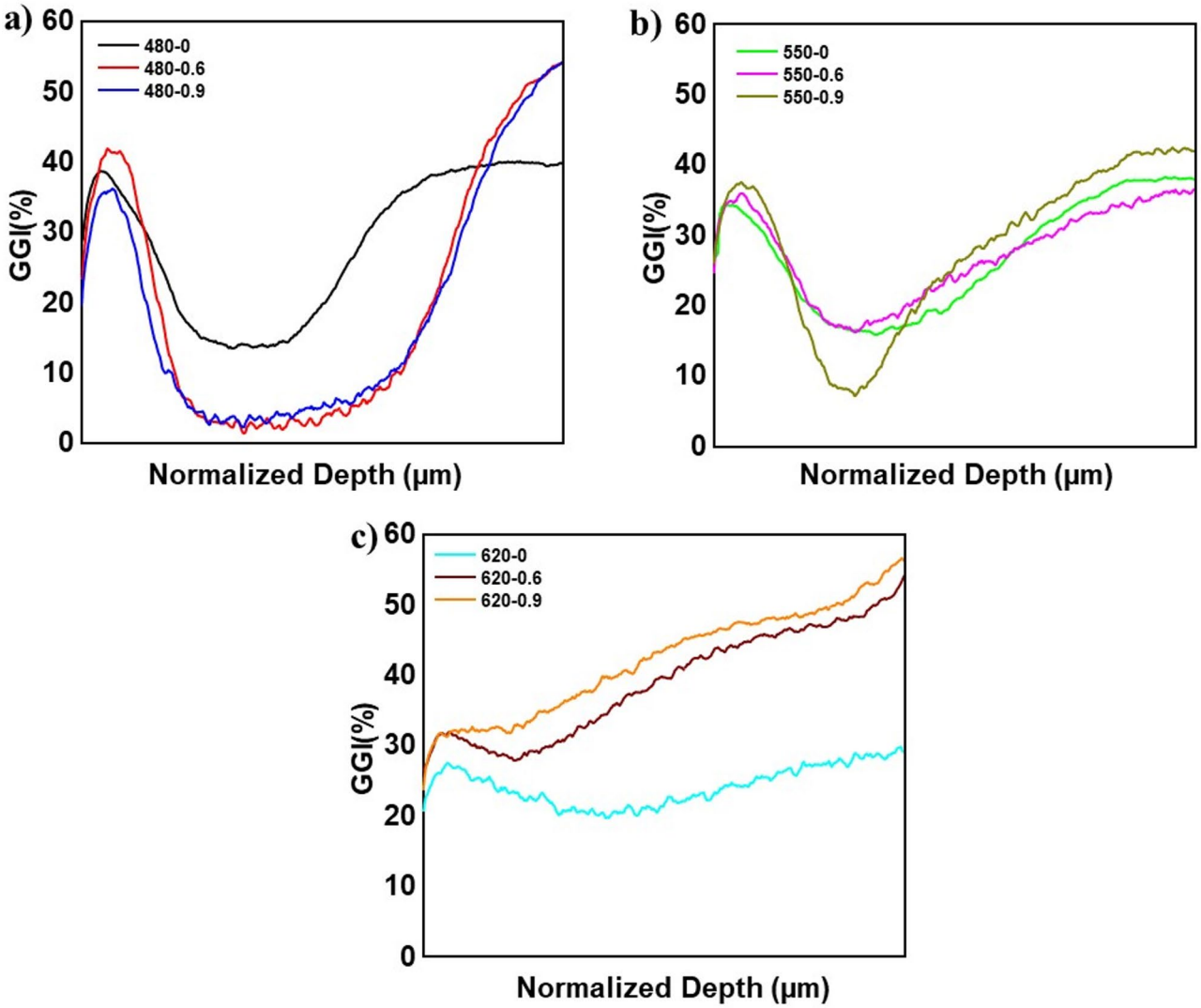

Fig. 4. Effect of Te addition and substrate temperature on the *GGI* gradient of samples. The left side of the graphs is the front interface with the CdS layer, and the right side is the Mo back contact.

mechanism leading to high-efficiency thin-film solar cells is not yet possible in the early stages of our experiments, we believe that further clarifications regarding the effects of elevated T_{Sub} and excess tellurium concentration will facilitate the establishment of guidelines for the development of both higher-efficiency thin-film solar cells and enhanced cell stability.

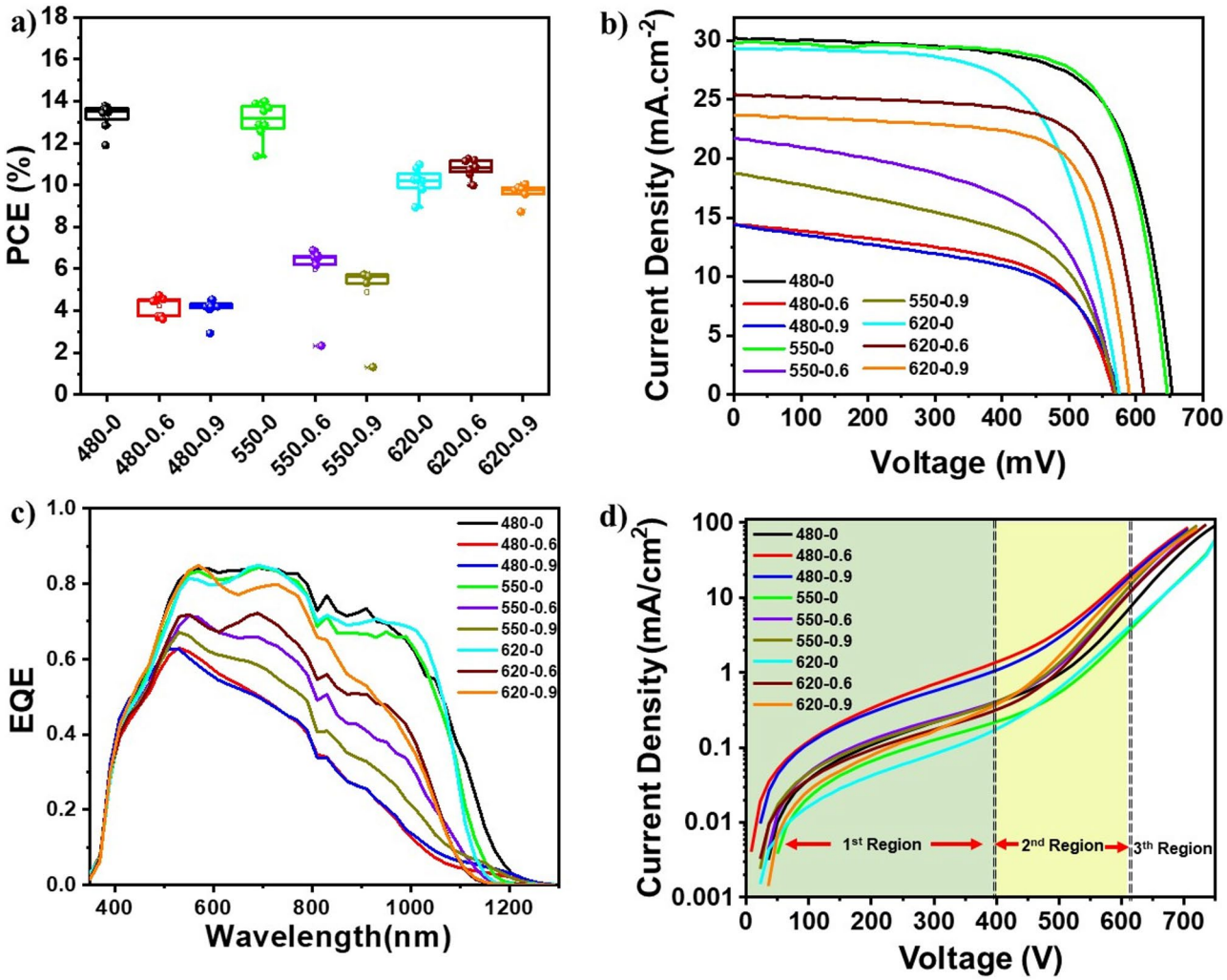

Fig. 5. (**a**) Statistical distribution of PCE of cells made with different Te concentration and substrate temperature, (**b**) *J-V* curves, (**c**) *EQE* graphs, and (**d**) Dark *J-V* curves of the best-performing cells for all samples.

Sample	J_{SC} (mA/cm^2)	V_{OC} (mV)	FF (%)	PCE (%)
480 – 0	31.01	654	69.6	14.12
480 – 0.6	16.95	567	57.8	5.55
480 – 0.9	17.19	574	55.0	5.43
550 – 0	29.83	647	72.6	14.01
550 – 0.6	22.00	569	55.6	6.96
550 – 0.9	19.52	570	53.7	5.97
620 – 0	30.11	575	65.1	11.27
620 – 0.6	23.58	612	72.2	10.42
620 – 0.9	26.42	590	71.8	11.19

Table 2. Solar cell parameters of the best solar cells for each sample.

Data availability

The datasets used and/or analysed during the current study available from the corresponding author on reasonable request.

Received: 28 May 2025; Accepted: 28 October 2025
Published online: 27 November 2025

References

1. Lundberg, O., Edoff, M. & Stolt, L. The effect of Ga-grading in CIGS thin film solar cells. *Thin Solid Films*. **480–481**, 520–525 (2005).
2. Guillemoles, J. F. The puzzle of Cu(In,Ga)Se2 (CIGS) solar cells stability. *Thin Solid Films*. **403–404**, 405–409 (2002).
3. Theelen, M. & Daume, F. Stability of Cu(In,Ga)Se2 solar cells: A literature review. *Sol Energy*. **133**, 586–627 (2016).
4. Naghavi, N. et al. Ultrathin Cu(In,Ga)Se2 based solar cells. *Thin Solid Films*. **633**, 55–60 (2017).
5. Zahedi-Azad, S., Maiberg, M. & Scheer, R. Effect of Na-PDT and KF-PDT on the photovoltaic performance of wide bandgap Cu (In,Ga)Se2 solar cells. *Prog Photovolt. Res. Appl.* **28**, 1146–1157 (2020).
6. Gloeckler, M. & Sites, J. R. Band-gap grading in Cu(In,Ga)Se2 solar cells. *J. Phys. Chem. Solids*. **66**, 1891–1894 (2005).
7. Witte, W. et al. Gallium gradients in Cu(In,Ga)Se2 thin-film solar cells. *Prog Photovolt. Res. Appl.* **23**, 717–733 (2015).
8. Wei, S. H., Zhang, S. B. & Zunger, A. Effects of Ga addition to CuInSe2 on its electronic, structural, and defect properties. *Appl. Phys. Lett.* **72**, 3199–3201 (1998).
9. Yetkin, H. A. et al. Decay mechanisms in CdS-buffered Cu(In,Ga)Se2 thin-film solar cells after exposure to thermal stress: Understanding the role of Na. *Prog Photovolt. Res. Appl.* **29**, 1034–1053 (2021).
10. Agca, S., Çankaya, G. & Sonmezoglu, S. Impact of tellurium as an anion Dopant on the photovoltaic performance of wide-bandgap Cu(In,Ga)Se2 thin-film solar cells with rubidium fluoride post-deposition treatment. *Front. Energy Res.* **11**, 1215712. https://doi.org/10.3389/fenrg.2023.1215712 (2023).
11. Mise, T. & Nakada, T. Effect of tellurium deposition rate on the properties of Cu–In–Te based thin films and solar cells. *J. Cryst. Growth*. **314**, 76–80 (2011).
12. Ishizaki, T., Saito, N. & Fuwa, A. Electrodeposition of CuInTe2 film from an acidic solution. *Surf. Coat. Technol.* **182**, 156–160 (2004).
13. Roy, S., Bhattacharjee, B., Kundu, S., Chaudhuri, N., Pal, A. K. & S. & Characterization of CuInTe2 thin film synthesized by three source co-evaporation technique. *Mater. Chem. Phys.* **77**, 365–376 (2003).
14. Wasim, S. M. et al. Effect of localized modes in the absorption spectra of CuInTe2, CuIn3Te5 and CuIn5Te8. *J. Phys. Chem. Solids*. **64**, 1995–2000 (2003).
15. Aissaoui, O. et al. Study of flash evaporated CuIn1-xGaxTe2 (x = 0, 0.5 and 1) thin films. *Thin Solid Films*. **517**, 2171–2174 (2009).
16. Fiat, S. et al. The influence of stoichiometry and annealing temperature on the properties of CuIn0.7Ga0.3Se2 and CuIn0.7Ga0.3Te2 thin films. *Thin Solid Films*. **545**, 64–70 (2013).
17. Fiat, S., Polat, I., Bacaksiz, E., Kompitsas, M. & Çankaya, G. The influence of annealing temperature and tellurium (Te) on electrical and dielectrical properties of Al/p-CIGSeTe/Mo Schottky diodes. *Curr. Appl. Phys.* **13**, 1112–1118 (2013).
18. Fiat, S., Bacaksiz, E., Kompitsas, M. & Çankaya, G. Temperature and tellurium (Te) dependence of electrical characterization and surface properties for a chalcopyrite structured Schottky barrier diode. *J. Alloys Compd.* **585**, 178–184 (2014).
19. Varol, S. F., Bacaksiz, E., Koralli, P., Kompitsas, M. & Çankaya, G. A novel nanostructured CuIn0.7Ga0.3(Se0.4Te0.6)2/SLG multinary compounds thin films: for photovoltaic applications. *Mater. Lett.* **142**, 273–276 (2015).
20. Fiat, S. et al. Optical and structural properties of nanostructured CuIn0.7Ga0.3(Se(1 – x)Te x)2 chalcopyrite thin films-Effect of stoichiometry and annealing. *J. Nanosci. Nanotechnol.* **14**, 5002–5010 (2014).
21. Atasoy, Y. et al. Cu(In,Ga)(Se,Te)2 pentenary thin films formed by reaction of precursor layers. *Thin Solid Films*. **592**, 189–194 (2015).
22. Mise, T. & Nakada, T. Low temperature growth and properties of Cu–In–Te based thin films for narrow bandgap solar cells. *Thin Solid Films*. **518**, 5604–5609 (2010).
23. Mise, T. & Nakada, T. Microstructural and optical properties of CuIn3Te5 thin films for solar cells. *Sol Energy Mater. Sol Cells*. **94**, 1132–1136 (2010).
24. Herberholz, R. & Carter, M. J. Investigation of the chalcogen interdiffusion in CuIn(TeSe)2 thin films. *Sol Energy Mater. Sol Cells*. **44**, 357–366 (1996).
25. Jehl-Li-Kao, Z., Kobayashi, T. & Nakada, T. CuIn(Se1 – xTex)2 solar cells with tunable narrow-bandgap for bottom cell application in Multijunction photovoltaic devices. *Sol Energy Mater. Sol Cells*. **119**, 144–148 (2013).
26. Atasoy, Y. et al. In,Ga)(Se,Te)2 films formed on metal foil substrates by a two-stage process employing electrodeposition and evaporation. *Thin Solid Films* **649**, 30–37 (2018).
27. Agca, S. & Çankaya, G. Effect of gallium content on diode characteristics and solar cell parameters of Cu(In1-xGax)(Se0.98Te0.02)2 thin film solar cells produced by three-stage co-evaporation at low temperature. *GU J. Sci. Part. C.* **11**, 1108–1115 (2023).
28. Agca, S. & Çankaya, G. Photovoltaic properties of Cu(In,Ga)(Se,Te)2 thin film solar cells with different tellurium amounts and a copper-poor stoichiometry. *Int. J. Energy Stud.* **8**, 849–858 (2023).
29. Jarzembowski, E. et al. Optical and electrical characterization of Cu(In,Ga)Se2 thin film solar cells with varied absorber layer thickness. *Thin Solid Films*. **576**, 75–80 (2015).
30. Kodalle, T. et al. Glow discharge optical emission spectrometry for quantitative depth profiling of CIGS thin-films. *J. Anal. Spectrom.* **34**, 1233–1241 (2019).
31. Okuyama, K., Tsuhako, J. & Kumagai, Y. Behavior of metal contacts to evaporated tellurium films. *Thin Solid Films*. **30**, 119–126 (1975).
32. Diaz, R., Leon, M. & Rueda, F. Characterization of Cu–In–Se–Te system in thin films grown by thermal evaporation. *J. Vac Sci. Technol. A*. **10**, 295–300 (1992).
33. Sonmezoglu, S. & Akman, E. Improvement of physical properties of ZnO thin films by tellurium doping. *Appl. Surf. Sci.* **318**, 319–323 (2014).
34. Akin, S., Erol, E. & Sonmezoglu, S. Enhancing the electron transfer and band potential tuning with long-term stability of ZnO based dye-sensitized solar cells by gallium and tellurium as dual-doping. *Electrochim. Acta*. **225**, 243–254 (2017).
35. Sonmezoglu, S., Termeli, T. A., Akın, S. & Askeroglu, I. Synthesis and characterization of tellurium-doped CdO nanoparticles thin films by sol–gel method. *J. Sol-Gel Sci. Techn*. **67**, 97–104 (2013).
36. Sonmezoglu, S. Synthesis and characterisations of nanostructured TiO2-Te:CdO compound thin films. *Mater. Technol.* **29**, 3–7 (2014).
37. Sharma, I., Pawar, P. S., Yadav, R. K., Nandi, R. & Heo, J. Review on bandgap engineering in metal-chalcogenide absorber layer via grading: A trend in thin-film solar cells. *Sol Energy*. **246**, 152–180 (2022).
38. Schneider, T., Dethloff, C., Hölscher, T., Kempa, H. & Scheer, R. Comparison of mo and ITO back contacts in CIGSe solar cells: vanishing of the main capacitance step. *Prog Photovolt. Res. Appl.* **30**, 191–202 (2022).
39. Orgis, T., Maiberg, M. & Scheer, R. Influence of band gradients on Cu(In,Ga)Se2 solar cell diode factors. *J. Appl. Phys.* **114**, 214506. https://doi.org/10.1063/1.4840995 (2013).
40. Nwakanma, O., Subramaniam, V. & Morales-Acevedo, A. Review on the effects due to alkali metals on copper–indium–gallium–selenide solar cells. *Mat. Today Energy*. **20**, 100617. https://doi.org/10.1016/j.mtener.2020.100617 (2021).
41. Liu, W. et al. Highly efficient CIGS solar cells based on a new CIGS bandgap gradient design characterized by numerical simulation. *Sol Energy*. **233**, 337–344 (2022).

Acknowledgements

This study is derived from the 'PhD Thesis' of the first author (S.A) in Ankara Yıldırım Beyazıt University, In-

stitute of Natural and Applied Science. This work was supported by The Scientific and Technological Research Council of Turkey (TUBITAK); and the Federal Ministry of Education and Research of Germany [Grant number 0324297B].

Author contributions

SA performed the fabrication and the characterization experiments. SA, HAY, and SS wrote the main manuscript text. GC supervised the study. All authors reviewed the manuscript.

Declarations

Competing interests

The authors declare no competing interests.

Additional information

Correspondence and requests for materials should be addressed to S.A.

Reprints and permissions information is available at www.nature.com/reprints.

Publisher's note Springer Nature remains neutral with regard to jurisdictional claims in published maps and institutional affiliations.